Subsurface defect characterization in artworks by quantitative PPT and holographic interferometry

by C. Ibarra-Castanedo*, S. Sfarra**, D. Ambrosini**, D. Paoletti**, A. Bendada* and X. Maldague*,

**Computer Vision and Systems Laboratory, Department of Electrical and Computer Engineering, 1065, av. de la Médecine, Laval University, Quebec City, Canada, G1V 0A6; {IbarraC, Bendada, MaldagX}@gel.ulaval.ca*
*** LAS.E.R. Laboratory, Department of Mechanical, Management and Energy Engineering (DIMEG), University of L'Aquila, Loc. Monteluco di Roio, 67040 Roio Poggio (AQ), Italy, {sfarra, dario}@ing.univaq.it*

Abstract

In this study, experimental data from two artwork specimens was acquired and processed by pulsed phase thermography (PPT) and holographic interferometry. The first specimen was a wood painting with a variety of damages typical of this kind of pieces. A comparative study between thermography and interferometry results showed the potential complementarities of both techniques. The second inspected specimen was a fresco with fabricated inserts inspected by PPT to detect and characterize the subsurface defects. The well-known concept of Signal-to-Noise Ratio (SNR) is proposed for the selection of the proper phasegram frequency at which defect sizing is performed. A de-noising step was required prior to the application of the Canny edge detection algorithm. It is demonstrated with this investigation that PPT and holographic interferometry are valuable tools for the qualitative and quantitative assessment of artworks.

1. Introduction

Cultural heritage pieces such as frescoes and other artworks of historical interest are highly sensitive to environmental conditions such as temperature, humidity and air pollutants. Non-invasive inspection techniques are required to diagnose the state of an artwork piece. Optical inspection techniques such as holographic interferometry have proven very effective in providing precise information about the size and location of defects [1]. Nevertheless, holographic techniques are difficult to apply in situ principally because of the strict stability requirements and high costs. The technique of electronic speckle pattern interferometry (ESPI) constitutes an interesting alternative [1]. Another possibility is to use infrared thermography, which is a non-contact, non-invasive and nondestructive evaluation (NDE) method [2]. However, problems such as non-uniform heating, emissivity variations, environmental reflections and surface geometry have a great impact on raw thermal data [3]. The phase delay data obtained by pulsed phase thermography (PPT) [4] is of great interest in NDE given that it is less affected than raw thermal data by all these problems [5], making of PPT a very attractive diagnosis tool not only for qualitative inspections but also for quantitative characterization of materials. The use of the phase from PPT in combination with the signal-to-noise ratio (SNR) is investigated for the determination of the size and depth of fabricated subsurface defects in a fresco sample. Integrated diagnostics with holographic interferometry (HI) is also discussed.

2. Pulsed phase thermography

Pulsed thermography (PT) is one of the simplest, fastest and more popular active thermography techniques [2]. PT is however affected by a variety of problems such as reflections from the environment, emissivity variations, non-uniform heating and surface geometry variation [4], [5]. The use of processing techniques can considerably reduce the impact of some or all of these problems: thermal contrast, differential absolute contrast (DAC), principal component thermography (PCT), thermographic signal reconstruction (TSR), among others. References [6], [7], [8] describe these techniques in detail.

Pulsed phase thermography (PPT) is another interesting processing technique well described in the literature [4], [9], [10]. As a recall, Figure 1a depicts the acquisition and data processing steps involved in PPT. A synchronization unit is needed to control the time between the launch of the thermal pulse and the recording. Data is stored as a 3D matrix as depicted in Figure 1b, where x and y are the spatial coordinates, and t is the time. The temperature of a point on the surface decreases at a rate that can be approximated by the square root of time ($t^{1/2}$), at least at early times, except for the defective areas, where the cooling rate is different as seen in Figure 1d. The 1D fast Fourier transform algorithm is applied pixel by pixel, providing a 3D complex matrix from which the amplitude and phase delay data can be retrieved. Figure 1c portrays the 3D phase matrix reconstructed from pulsed data using the fast Fourier transform algorithm. The phase profiles for a defective pixel (red) and a non-defective (blue) one are shown in Figure 1e.

The main interest of the PPT technique is the estimation of the phase delay information given that phasegrams are less affected than raw thermograms by the typical problems mentioned before. These phase characteristics are very attractive not only for qualitative inspections but also for quantitative characterization of materials. For instance, a depth inversion technique using the phase from PPT has been proposed [11], [12]. The technique relies on the thermal diffusion length equation, *i.e.* $\mu=(\alpha/\pi \cdot f)^{1/2}$, in a manner similar to lock-in thermography [13]. Nevertheless, as it is well-known [14], noise content present in phase data is considerable, especially at high frequencies. This causes a problem for the determination of the blind frequency. A de-noising step is therefore often required. The combination of PPT and TSR has proven to be very effective for this matter,

reducing noise and allowing the depth retrieval for a defect [15]. Another difficulty is that, given the time-frequency duality of the Fourier transform, special care must be given to the selection of the sampling and truncation parameters prior to the application of the PPT. These two parameters depend on the thermal properties of the material and on the depth of the defect, which are often unknown. An interactive procedure has been proposed [16].

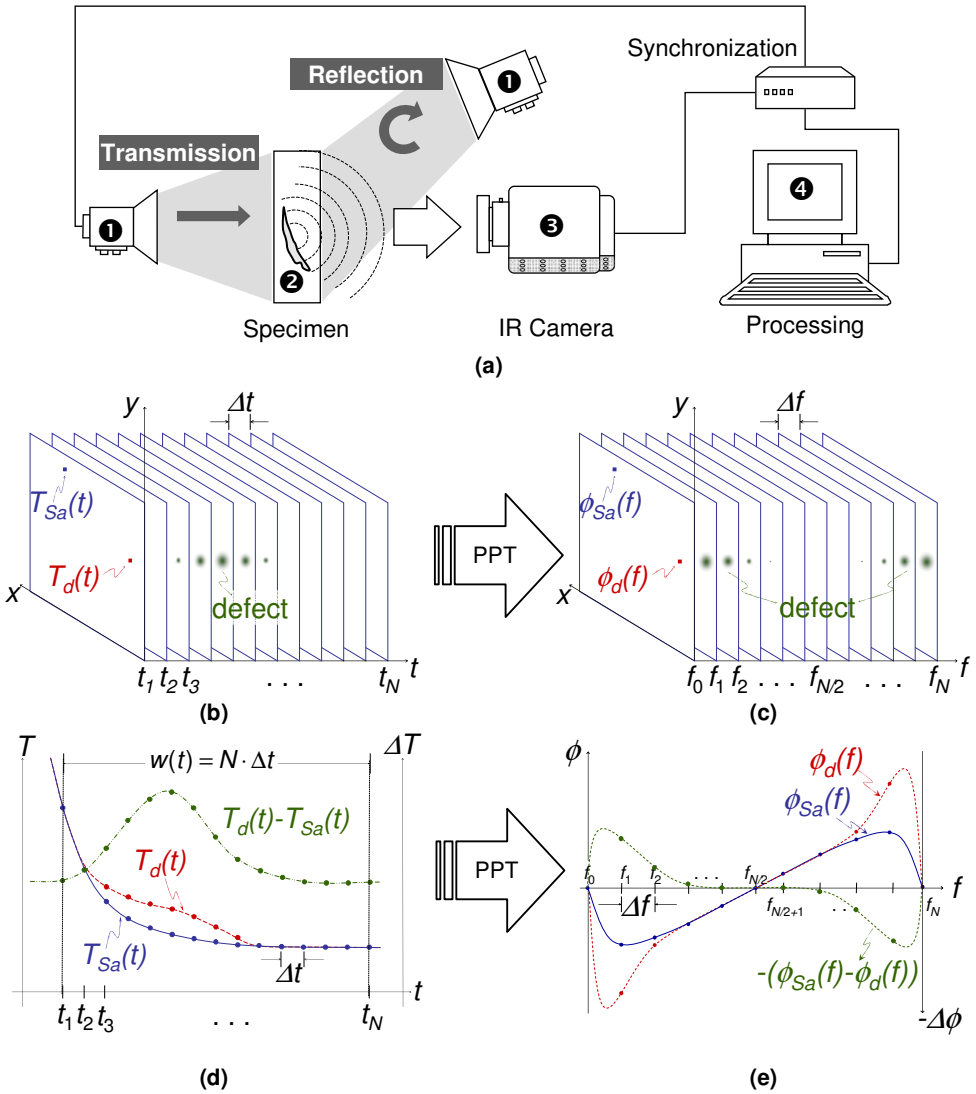

Figure 1. Data acquisition and signal processing in PPT: (a) four steps for data acquisition, (b) thermogram 3D matrix depicting the appearance and disappearance of a defect through time, (c) phasegram 3D matrix showing the defect visibility in the frequency spectrum, (d) thermal profiles for a defective pixel (–T_d), a non-defective pixel (--T_{Sa}) and the difference between them (-·-T_d -T_{Sa}), and (e) phase profiles for a defective pixel (–ϕ_d), a non-defective pixel (--ϕ_{Sa}) and the difference between them (-·-ϕ_d -ϕ_{Sa}).

3. Holographic Interferometry (HI)

Holographic Interferometry (HI) is a well known tool in NDE [17]. The basic goal of HI is the comparison of an object of interest with itself under different operating conditions. Holographic interferometry has three basic variations: single exposure, double exposure and sandwich holography; each possessing certain advantages over the other in particular test situations [1], [18]. Real time HI involves the recording of a conventional hologram of the investigated test object, the exact reposition of this hologram in the same position in which it was recorded and the live observation of the formation and evolution of the interference fringes. The main feature of single exposure HI lies in its dynamic nature: the phenomena can be followed in time. The main disadvantages are the reduced fringe contrast (in comparison with double exposure HI) and some practical difficulties, *e.g.* hologram must be repositioned with a precision in the order of wavelength.

In double exposure HI two holograms are recorded on the same plate, with each one capturing the object in a different state separated by a fixed time interval. This technique is less critical than real time holography, because the two interfering waves are always reconstructed in exact register, and the fringes have a good contrast. However, double exposure HI is not dynamic and information on intermediate states of the test object is lost.

Sandwich holography or, more precisely sandwich HI is a particular ingenious form of holographic interferometry based on the concept of recording two exposures on different plates.. This technique gives more versatility to the double exposure set up; instead of making a double exposure on one holographic plate, the two exposures are made on different plates which are, then, combined in a plate holder. The image, reconstructed from a sandwich hologram gives the same fringes of a conventional double exposure hologram but, by having the images on two different plates, it is possible to manipulate them, by shifting and tilting, and hence the fringe pattern.

There are several advantages in using this version of HI. For example, a number of holograms can be made, each one recording a single state of the test section, in a temporal sequence. Afterwards the plates can be combined in pairs as desired, allowing one to compare any two hologram plates to study interferometrically any changes in the test object, in order to have a *quasi* continuous monitoring of the deformation. Probably the most important advantage of sandwich holography is the possibility to eliminate unwanted fringes, caused by rigid body motion of the object investigated, with an *a posteriori* manipulation of the fringe pattern [18]. There are of course some disadvantages: the plates have to be repositioned with high accuracy during reconstruction; the freedom of fringe manipulation also contains the seeds of possible errors. A correct use of the technique generally requires a specially designed holographic plate holder.

Because of its extreme sensitivity to surface deformation, holographic interferometry can be used to gain meaningful information with regard to the structural characteristics of an object, by observing the surface movement produced when it is subjected to a stressing force; as such it offers the potential for many nondestructive inspections wherein the parameter of interest, (cracks, voids, detachments) can be made manifest as discontinuities in surface displacement; the discontinuities appear as an anomaly in an otherwise regular interferometric fringe pattern and hence enable the region of fault to be identified. For this reason a stressing technique must be devised in such a way that the anomalies induce detectable perturbations in the surface deformation; usually the stressing method (a temperature gradient obtained by heating the surface by an infrared lamp or a stream of moderately warm air) is chosen empirically with guidance provided by an analysis of anticipated deformation and by previous results obtained from programmed models. Generally, artworks are analysed in thermal drift (with a short thermal irradiation which raises the surface temperature of some degrees) or in ambient drift (under ambient parameter variations). It seems that the thermal-drift method is considerably better in detecting detached regions.

A major problem that prevents the diffusion of the technique is the need to transport the artwork to an optical laboratory. In fact, the practical application of holographic interferometry has some disadvantages, which have, in general, hindered its widespread use *in situ*. To obtain a holographic interference pattern of good quality, the experimental set up must remain stable within fraction of a μm. Due to these stringent stability requirements, standard holographic techniques are usually performed on vibration-isolated heavy tables. Holography could be performed *in situ* using pulsed lasers but in this case there are problems because of size, weight and cost of the system and the need of special safety precautions. Some shortcomings of HI can be overcome, at the expense of a decrease in sensitivity and image quality, introducing two different speckle techniques: ESPI and speckle decorrelation [18].

4. Comparative study of a wood specimen by pulsed phase thermography and sandwich HI

4.1 Experimental setup and data acquisition

The PPT data acquisition configuration for the first sample is presented in Figure 2a. The specimen was heated during 13 minutes using 3 lamps (250 W / lamp), and the surface cooling down was recorded with an IR camera. One thermogram was acquired every 30 s and the acquisition lasted for 30 minutes, providing 48 thermograms. Front and rear surfaces views are seen in Figure 2b and c, respectively. The thermography inspected area only covers one of the nailed slabs as seen in Figure 2c and Figure 3. References to other defects discussed on the results section of the paper are also included: defect "A" consisting on a surplus material apparently after insertion and extraction of a nail from the back side (see magnified area in Figure 2c); defect "D", which is the interface between the two wood plates used for the painting, and a group of defects denoted as "N", which are 4 nail marks from one of the slabs.

HI experiments were carried out with a traditional holographic interferometry setup [1], [17] but using a special plate holder to perform sandwich HI. The specimen was briefly heated by moderately warm air raising surface temperature of about 2°C. The first hologram was recorded with the specimen at thermal equilibrium, then specimen was heated and successive holograms were recorded during the cooling process.

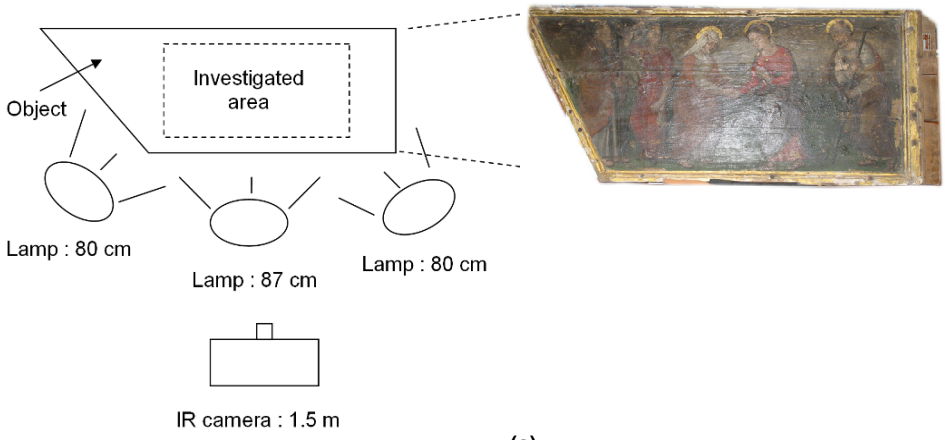

(a)

(b)

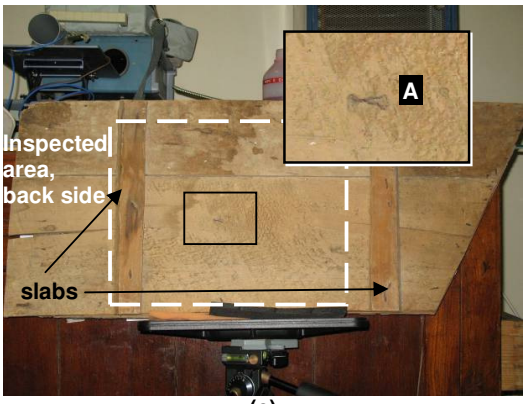

(c)

Figure 2. (a) Experimental setup used to inspect the wood specimen by infrared thermography, and photographs showing the: (b) front side, and (c) back side of the wood specimen and square area magnification showing defective area "A".

4.2 Results

The location of the interface between plates is indicated in Figure 3a; the top wood plate was infected with woodworms as shown in Figure 3b; and four nails on one side of the painting are identified, defect "N" in Figure 3c. Figure 4 presents a detailed view of the woodworms damaged area. In addition, it is possible to identify a small surface scratch, defect "L" (Figure 4a) and the surface porosity (small holes and cracks) caused by the woodworms (Figure 4b).

Figure 5a presents a photograph of the specimen showing the areas inspected by HI (white rectangle) and by PPT (black rectangle). Sandwich holograms can be obtained by shifting of the plates in such a way that different fringe systems can be produced, thus performing a continuous “scanning” of the deformation field. Figure 5b shows a holographic result in which the following subsurface features can be detected: the interface between plates ("D"), the surplus material ("A"), a scratch ("L") and two defects ("B" and "C") that correspond to porosity damaged areas caused by the presence of woodworms. One of the 4 nails ("N") is clearly detected, 2 other nails are slightly seen and the bottommost nail was not covered in the HI inspected area. Figure 5c presents a photograph of the rectangular area depicted in the holographic result of Figure 5b. The magnified area is shown in Figure 5d. The fusion of these two images is presented in Figure 5e, in which there is clearly seen that these two defects correspond to two cracks. It is interesting to note that although there are many other similar and even larger defects in the painting, see for instance defect marked as "F" in Figure 5, holographic results provide a very good indication of cracks "B" and "C". The small holes such as defect "F" however, although seen in the holographic image, do not produce a distorted fringe pattern.

Figure 5f and g present two phasegrams at different frequencies. Figure 5f, showing a low frequency phasegram (1.2 mHz), allows detecting subsurface features such as the interface between plates ("D"), the 4 nails ("N"), the surplus material ("A"), a scratch ("L") and many small holes such as defect "F". The higher frequency phasegram (3.5 mHz) in Figure 5g, besides of showing this same features (with more or less detail than the low frequency phasegram), some surface characteristics can also be observed, such as the emissivity variations caused by the painting and the porosity of the top wood plate. Defects "B" and "C" are not clearly identified by PPT, only the small hole near to crack defect "C" can be identified but none of the cracks.

Comparing results of both techniques in Figure 5 it can be observed that the interface between plates ("D") and the surplus materials ("A") probably caused by the extraction of a nail (see magnified area in Figure 2c) are clearly detected by both techniques. Nevertheless, some features such as the surface scratch ("L"), the nails ("N") and the small holes all over the painting (*e.g.* defect "F") are more evident in the PPT result. On the contrary, defects "B" and "C", which correspond to two surface cracks, are easily identified by holography. This situation provides an insight on the complementary capabilities of both techniques for the inspection of artworks.

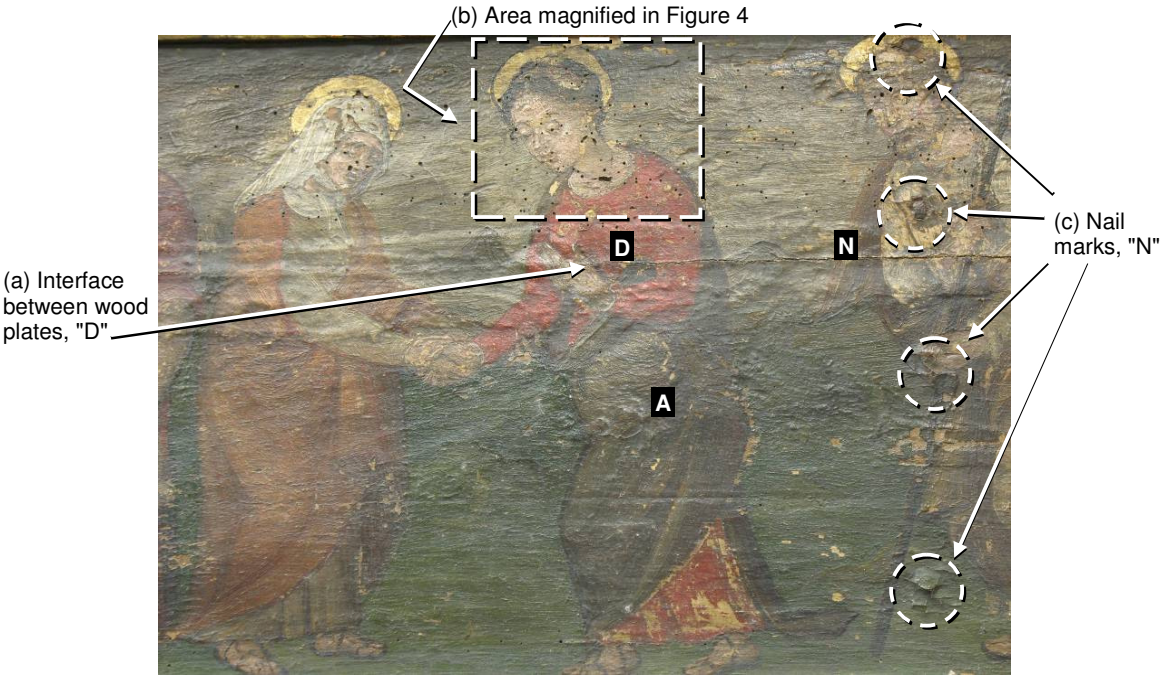

Figure 3. Photograph of the inspected area showing details about: (a) the location of the interface between the wood plates, "D"; (b) the location of the area magnified in Figure 4, and (c) the four nails in the right slab, "N".

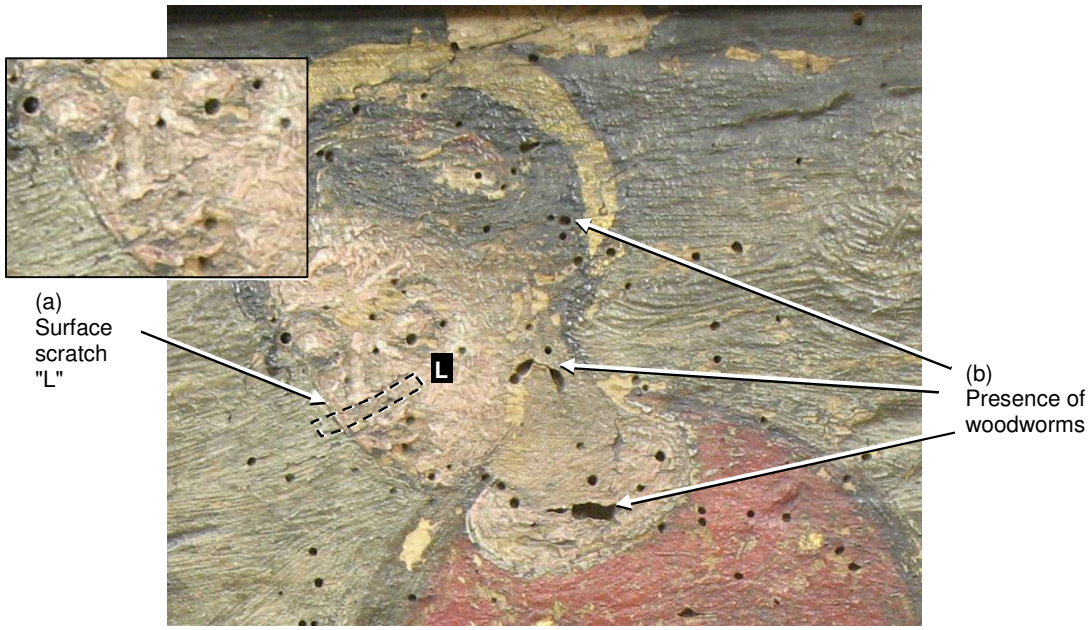

Figure 4. Rectangular area depicted in Figure 3b showing details: (a) surface scratch, "L"; and (b) damage caused by the presence of woodworms.

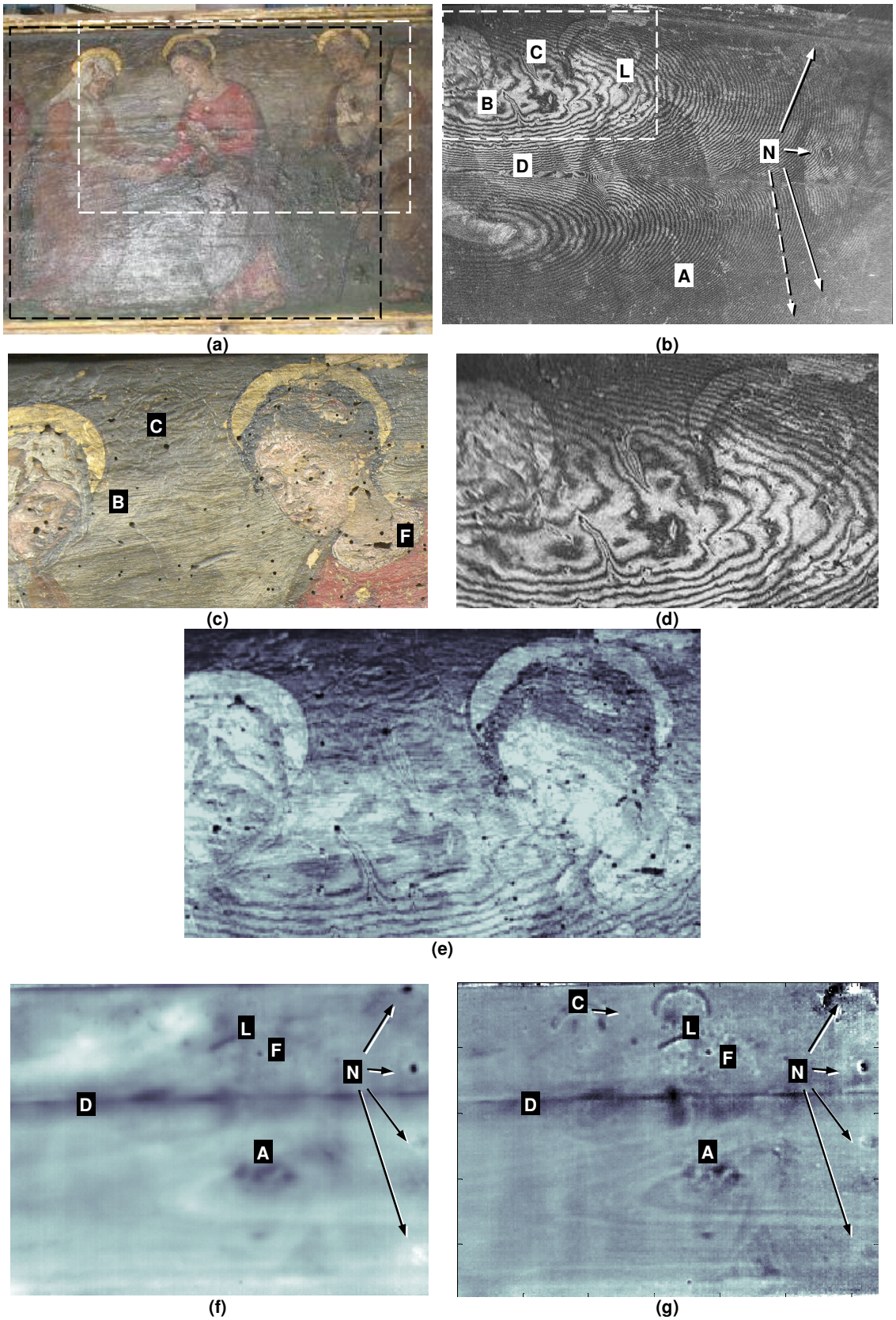

Figure 5. (a) Photograph of the specimen showing the areas inspected by HI (white rectangle) and by PPT (black rectangle), (b) sandwich hologram result of the HI inspected area, (c) photograph of the specimen covering the rectangular area depicted in (b), (d) magnification of the rectangular area depicted in (b) showing defect "B" and "C", and (e) fusion of images in (e) and (f), and phasegrams of the PPT inspected area at (c) 1.2 mHz and (d) 3.5 mHz.

5. Quantitative characterisation of a fresco by pulsed phase thermography

5.1 Experimental setup and data acquisition

Figure 6 shows the data acquisition configuration. The specimen was heated during 13 minutes using 3 lamps (250 W / lamp), and the surface cooling down was recorded with an IR camera. One thermogram was acquired every 30 s and the acquisition lasted for 3630 s (*i.e.* 1 hour and 30 s), providing 121 thermograms. The fresco specimen was manufactured with non-homogeneous materials to simulate the background irregularities typical of ancient walls. Four defects were inserted: two air voids and two sponge inserts with the characteristics described in Table 1.

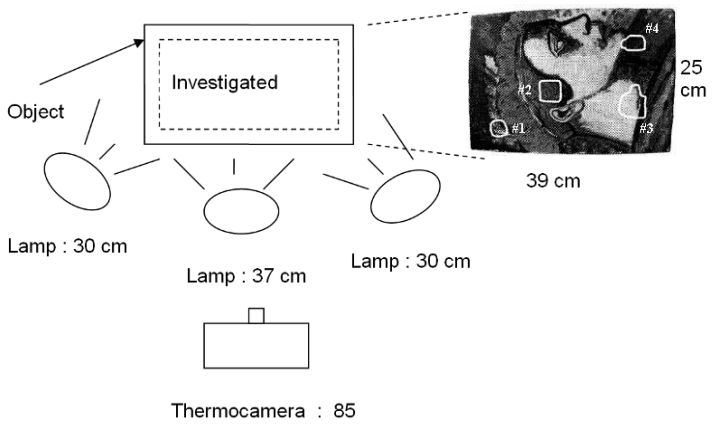

Figure 6. Experimental setup for data acquisition by pulsed thermography and the pictorial layer of the fresco showing the approximate defect locations.

The exact defect dimensions from the manufacturer are only available for the two air defects (defects D2 and D3 shown in Figure 7c). Nevertheless, the estimated dimensions, depths and thicknesses for all 4 defects, available in reference [19] are included in Table 1 as guidelines.

As seen in Figure 7a, a fresco is composed of different layers: the pictorial layer (Figure 7b), the mortar (Figure 7c), and the support wall (Figure 7d), which serves as a base for the painting. In the case of the inspected specimen, two artificial air voids were inserted in the mortar layer as seen in Figure 7c, and a crack, visible in the support wall (Figure 7d), was produced through artificial ageing of the support.

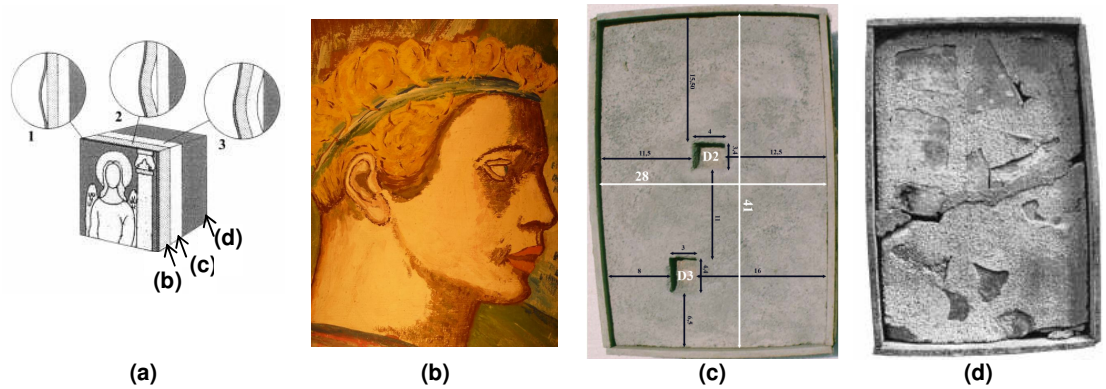

Figure 7. (a) Schematic representation of the different layers of the fresco, (b) pictorial layer of the fresco showing the approximate defect locations, (c) mortar with the location and dimensions of the air void defects (D2 and D3), and (d) support wall showing an artificially created crack. Images (a) and (d) from [19].

Table 1. Characteristics of the simulated defects in the fresco specimen (data adapted from references [19] and [20]).

Defect	Type	Dimensions [mm]	Depth* [mm]	Thickness* [mm]	Reported area [mm^2]	Estimated area [mm^2]	% error
D1	sponge insert	D=35 *	3	3	962	307	-68.1
D2	air void	40x34 **	7	5	1360	1146	-15.7
D3	air void	30x44 **	10	10	1320	1339	1.4
D4	sponge insert	45x45 *	10	15	2025	658	-67.5

*Estimated dimensions from reference [19].
** Real dimensions specified by the manufacturer (Figure 7c).

5.2 Results

Figure 8 shows three raw thermograms at different times. At early times (30 s in Figure 8a), the thermal signatures are related to the emissivity variations from the painting variations. Even though the emissivity variations still have an impact 300 s after heating (Figure 8b), it is possible at this point to have an indication of some of the defects. Dotted circles were added in Figure 8b to indicate the approximate locations of the four defects. This image is in fact the one providing the best overall defect visibility. At later times, defect contrast worsens as can be seen in Figure 8c for a thermogram 1920 s after heating.

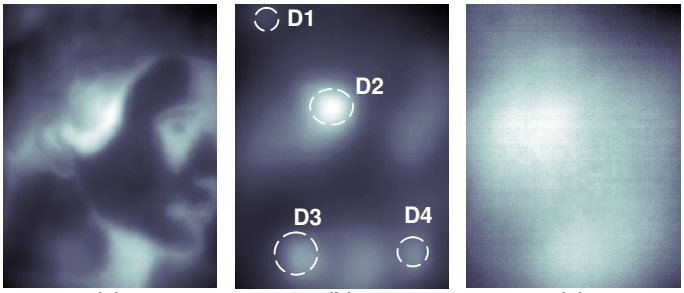

Figure 8. Raw thermograms at t=(a) 30 s, (b) 300 s, and (c) 1920 s..

PPT was chosen to provide phase images or *phasegrams*, which are less affected by undesirable optical and thermal artifacts. However, noise content in phasegrams is considerable [12], especially at high frequencies. Hence, data was first filtered in order to de-noise the signal and then processed by PPT providing phase delay data. The resulting phasegrams were then used to detect the defects. For every defect, the signal-to-noise ratio (SNR) was estimated as [20]:

$$\mathrm{SNR} = \frac{S_{def} - S_a}{\sigma_{S_a}} \qquad (1)$$

where S is the signal, the phase in this case, evaluated in a defective area $_{def}$ or a sound area $_{Sa}$, and σ_{Sa} is the standard deviation in the sound area. For a particular defect, the sound area was selected right next to it, calculated as the average value over the surface covered by the rectangular areas, see Figure 9a.

Applying this operation to the whole sequence allowed to determine the frequency of maximum SNR for every defect and to use this frequency for the segmentation and size estimation. Once the frequency of maximum SNR was determined for every defect, the Canny edge detection algorithm [21] was used to find the defects edges in the phasegram matrix. Figure 9b to d presents the results. The defect size was estimated by calculating the area inside the segmented regions.

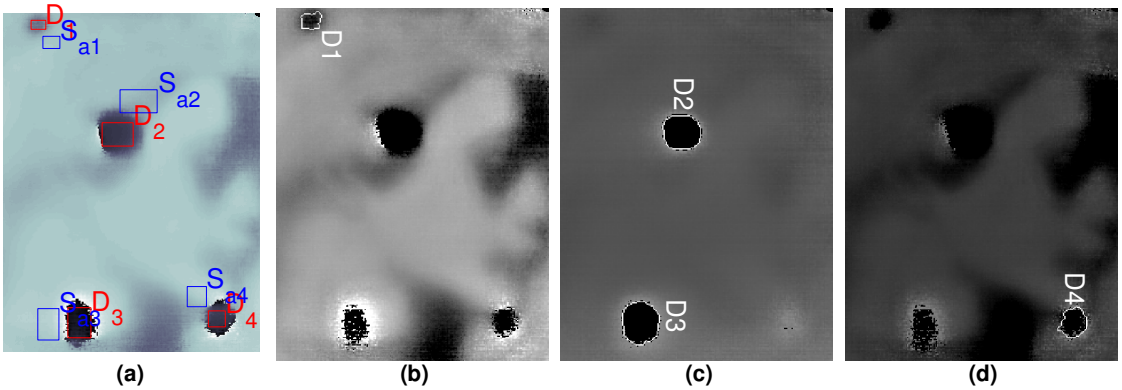

Figure 9. (a) Phasegram at f= 1 mHz showing the areas (defects and sound) used for the SNR calculations. Segmentation results: phasegrams at f=(b) 1 mHz, (c) 0.34 mHz and (d) 1.3 mHz.

Results of the estimated area and %error (with respect to the available information from the specimen manufacturer for defects D2 and D3, and to the estimated data from references [19] and [20] for defects D1 and D4) are presented in the last two columns of Table 1, respectively. Defect 1 (D1) presented a maximum SNR at 1 mHz, D2 and D3 at a lower frequency (0.34 mHz) and D4 at a higher frequency (1.3 mHz). From Table 1 it can be seen that defects D1 and D4 are the same type, *i.e.* sponge inserts, whilst defects D2 and D3 are both air voids. As a first observation, there is a relationship between the defect type and its corresponding frequency of maximum SNR: defects D1 and D4 have a better visibility at higher frequencies than defects D2 and D3. Another important observation is that, even though the reported dimensions of air voids defects (D2 and D3) are very

close (1360 mm^2 vs. 1320 mm^2), better sizing (error$_{D2}$=-15.7% vs. error$_{D3}$=1.4%error, see Table 1) is achieved for D3, *i.e.* the shallowest defect (z_{D2}=10 mm vs. z_{D3}=7 mm). The thickness variation (th_{D2}=10 mm vs th_{D3}=5 mm) had a lesser impact than the depth. In the case of sponge inserts (D1 and D4), the %error was estimated with respect to the evaluated dimensions of the sponge inserts as reported in references [19] and [20]. The %error is much larger in this case. According to the segmentation results presented in Figure 9, defects D1 and D4 have a quasi-circular shape of approximately 19.8 and 29 mm in diameter (307 and 658 mm^2), respectively, which correspond to considerably smaller defects than the estimations presented in previous works. In order to improve sizing estimation by PPT, it would be necessary to perform a new test with a shorter heating time, *e.g.* with high power flashes. In addition, it was observed that the defect thickness played a more important role (th_{D1}=3 mm vs. th_{D4}=15 mm), than the defects depth (z_{D1}=3 mm vs z_{D4}=10 mm) on defect detection. As discussed in section 2, high frequencies are related to shallow defects whilst low frequencies with deep defects. In this case however, the defect thickness had a greater impact on the phase given that the thickest (although shallowest) defect has its best SNR at a lower frequency than the thinnest (although deepest) sponge insert.

Figure 10 presents three images obtained by adding the photo of the fresco (seen in Figure 7b), a photo of the mortar layer showing the air voids locations (Figure 7c) and the phasegram at different frequencies. The defect location is superposed to the fresco photograph in Figure 10a. At f= 0.3 mHz (Figure 10b), the air voids (defects D2 and D3) and the bottom sponge insert (D4) can be detected and superimposed to Figure 10a. The sponge insert (D1) is visible only at f= 2.7 mHz. In this later frequency, the shape of the air voids is deformed since more superficial information, such as emissivity variations of the painting, is seen buy the phase.

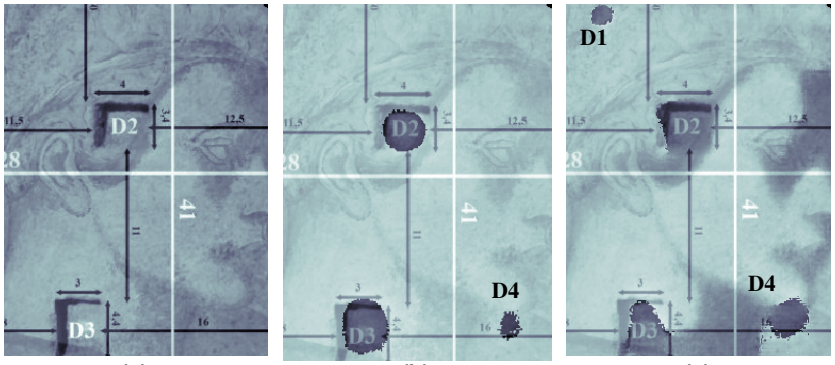

Figure 10. (a) Image fusion from the fresco photograph (Figure 7b) and the mortar layer (Figure 7c), image fusion between Figure 10a and phasegrams at f=(b) 0.3 mHz and (c) 2.7 mHz.

A higher frame rate could be used in order to improve results, this will provide more data points prior to the application of the PPT algorithm, increasing in this way the frequency and spatial resolutions.

5.3 Holographic interferometry

HI experiments were performed with a traditional holographic interferometry setup [1], [17] using double exposure HI. The specimen was heated using two lamps (150 W / lamp) at a distance of about 1 m raising surface temperature of about 3-4 °C. First exposure was recorded with the specimen at thermal equilibrium, then specimen was heated and second exposure was recorded during the cooling process. Choosing different times of second exposure gives rise to different fringe patterns, *i.e.* different detection of subsurface defects. Figure 11 shows a double exposure hologram where the simulated defects are clearly located. Furthermore, contrary to the thermographic results, a crack, arisen during the heating and cooling cycles of diagnostic experiments was detected.

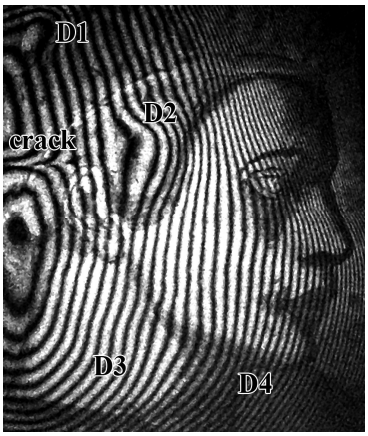

Figure 11. Double exposure holograms of the fresco specimen.

This defect does not correspond to the artificial crack in the support wall (Figure 7d), which is too deep to be detected by either holographic or thermography techniques. For a comparison with different double exposure holograms and ESPI results on the same artwork, see [17].

6. Conclusions

Infrared thermography and holographic interferometry were used to inspect two artwork samples. The first specimen was an ancient painting on wood. Data was acquired and stored for later processing using pulsed phase thermography. Results show that a variety of defects can be detected by both techniques. Some types of defects were more easily detected by one or other technique. For instance, although both techniques are able to detect a surface scratch and the nails marks, PPT results showed these features more clearly. On the other hand, holography provided good indications of cracks ("B" and "C") that were difficult to identify by PPT, and a non-fabricated crack (seen in Figure 11) on the fresco could only be detected by holographic means. The artificial crack located on the support layer is located to deep to be detected by HI or PPT. Nevertheless, alternative thermographic techniques, reported in the literature [22], [23], could provide suitable results for this kind of defects.

For the second specimen, PPT was used to detect and characterize fabricated defects on a fresco. It was observed that defect detection was straightforward on this study and defect characterization was dependent on the material used to simulate a defect. Air voids (defects D2 and D3), having a very low thermal diffusivity were more easily detected and characterized than the sponges (defects D1 and D4). Good agreement was observed between the estimated area for air void defects between this research and available data from the manufacturer previous works. The situation is different for the case of sponge defects, where area estimation results differ by almost a 70%. In order to better assess the sizing results by PPT it would be necessary to perform a new set of experiments using a shorter heating time. This will allow detecting defects at the cooling stage, and not during heating, which will improve defect characterization with the PPT phase delay information.

Acknowledgements

Authors want to thank the support of the *Chaire de recherche du Canada (MiViM)*, the *Ministère du développement économique, innovation et exportation du Québec* and the *Soprintendenza per i Beni Ambientali, Architettonici, Artistici e Storici per l'Abruzzo* (Italy) for granting permission to carry out experiments on the wooden panel *La Visitazione* (XVII century).

REFERENCES

[1] Paoletti D. and Schirripa Spagnolo G. "Interferometric methods for artworks diagnostics". *Progress in Optics* **XXXV**: 197-255, 1996.

[2] Nondestructive Handbook, Infrared and Thermal Testing, Volume 3, X. Maldague technical ed., P. O. Moore ed., 3rd edition, Columbus, Ohio, ASNT Press, 2001, 718 p.

[3] Maldague X. P. V. Theory and practice of infrared technology for nondestructive testing, John Wiley & Sons, N. Y., 2001.

[4] Maldague X. and Marinetti S. "Pulse Phase Infrared Thermography," *J. Appl. Phys,* **79**: 2694-2698, 1996.

[5] Busse G., Wu D. and Karpen W. "Thermal Wave Imaging with Phase Sensitive Modulated Thermography," *J. Appl. Phys*., **71**(8):3962-3965, 1992.

[6] Ibarra-Castanedo C., González D., Klein M., Pilla M., Vallerand S., Maldague X., "Infrared Image Processing and Data Analysis," *Infrared Physics and Technology*, **46**[1-2]: 75-83, 2004.

[7] Ibarra-Castanedo C., Genest M., Piau J.-M., Guibert S., Bendada A. and. Maldague X. P. V, "Chapter 16: Active infrared thermography techniques for the nondestructive testing of materials," in Ultrasonic and Advanced Methods for Nondestructive Testing and Material Characterization, C.H. Chen ed., 684p, World Scientific Publishing, May 2007.

[8] Ibarra-Castanedo C., Genest M., Servais P., Maldague X. and Bendada A. "Qualitative and quantitative assessment of aerospace structures by pulsed thermography", *NDT & E*, **22**(2-3):199-215, June-September 2007.

[9] Ibarra-Castanedo C. and Maldague X. "Pulsed phase thermography reviewed," *QIRT Journal*, **1**(1):47-70, 2004.

[10] Maldague X and Couturier J-P. "Review of Pulse Phase Infrared Thermography," *Proc. 4th International Workshop on Advanced Infrared Technology and Applications (AITA)*, Firenze, Italy, September 15-16, **53**(1):271-286, 1997.

[11] Ibarra-Castanedo C. "Quantitative subsurface defect evaluation by pulsed phase thermography: depth retrieval with the phase," *Ph. D. thesis*, Université Laval, 2005, [available online: http://www.theses.ulaval.ca/2005/23016/23016.pdf].

[12] Ibarra-Castanedo C., Avdelidis N. P., Grinzato E. G., Bison P. G., Marinetti S., Liu C. Genest M. and Maldague X. P. "Quantitative inspection of non-planar composite specimens by pulsed phase thermography," *Qirt Journal*, **3**(1):25-40, 2006.

[13] Meola C. and Carlomagno G. M. "Recent Advances in the Use of Infrared Thermography", *Meas. Sci. Technol*., **15**:27–58, 2004.

[14] Couturier J-P. and Maldague X., "Pulsed Phase Thermography of Aluminum Specimens", *Proc. SPIE*, **3056**:170-175, 1997.

[15] Ibarra-Castanedo C., Genest M., Servais P., Maldague X. and Bendada A., "Qualitative and quantitative assessment of aerospace structures by pulsed thermography," *NDT & E*, **22**(2 and 3):199-215, 2007.

[16] Ibarra-Castanedo C. and Maldague X. “Interactive methodology for optimized defect characterization by quantitative pulsed phase thermography,” *Research in Nondestructive Evaluation,* **16**(4):1-19, 2005.
[17] Vest C.M., *Holographic Interferometry*, Wiley, New York, 1979.
[18] Ambrosini D. and Paoletti D. "Holographic and speckle methods for the analysis of panel paintings. Developments since the early 1970s *", Reviews in Conservation* **5**: 38– 48, 2004.
[19] Schirripa Spagnolo G., Guattari G., Grinzato E., Bison P.G., Paoletti D. and Ambrosini D. *"*Frescoes diagnostics by electro-optic holography and infrared thermography" *NDT.net, The e-Journal of Nondestructive Testing & Ultrasonics*, **5**(1), 2000, [available online: http://www.ndt.net/article/v05n01/schirrip/schirrip.htm].
[20] Grinzato E. G., Bison P. G., Marinetti S., Liu C., Genest M. and Vavilov V. “Thermal NDE enhanced by 3D numerical modeling applied to works of art,” *15th WCNDT - World Conference on Nondestructive Testing*, [available online: http://www.ndt.net/article/wcndt00/papers/idn909/idn909.htm], Roma (Italy) 15-21 October 2000.
[21] Jain R., Kasturi R and Schunck B. G. *Machine Vision*, McGraw Hill, USA, 549 p., 1995.
[22] Gruss C. and Balageas D. "Theoretical and experimental applications of the flying spot camera," QIRT 92, Eurotherm Series 27, EETI ed., Paris 1992, pp. 19-24.
[23] Grinzato E., Bison P.G., Bressan C. and Mazzoldi A. "NDE of frescoes by Infrared Thermography and lateral heating," QIRT 98, Eurotherm Series 60, Lodz, Poland, 1998, pp. 64-67**.**